Local magnetic order in the vacancy-disrupted spin ice Ho_2TiO_5

Raju Baral [1,*] Haidong Zhou [2] Qiang Zhang [1] Benjamin A. Frandsen [3] and Stuart Calder [1,†]

[1]*Neutron Scattering Division, Oak Ridge National Laboratory, Oak Ridge, Tennessee 37831, USA*

[2]*Department of Physics and Astronomy, University of Tennessee, Knoxville, Tennessee 37996, USA*

[3]*Department of Physics and Astronomy, Brigham Young University, Provo, Utah 84602, USA*

(Received 2 July 2026; revised 27 August 2026; accepted 1 October 2026; published 16 October 2026)

We investigate how local magnetic correlations evolve when the classical pyrochlore spin ice $Ho_2Ti_2O_7$ is transformed into the partially disordered stuffed compound Ho_2TiO_5. Neutron scattering measurements were analyzed using real space magnetic pair distribution function, reciprocal space reverse Monte Carlo, and half-polarized neutron powder diffraction methods to connect the average crystal structure with local magnetic correlations. Both compounds retain long-range $Fd\bar{3}m$ symmetry, but in Ho_2TiO_5 the average structure does not fully capture the local Ho–O, Ti–O, and O–O bond-length disorder associated with partial Ho/Ti occupancy. Despite this disorder, half-polarized neutron powder diffraction shows that the Ho moments retain local ⟨111⟩ Ising anisotropy and form spin-in/spin-out configurations on the tetrahedral network. In $Ho_2Ti_2O_7$, real- and reciprocal-space analyses show a nearly ideal 2-in/2-out spin ice state at 0.3 K, with ∼95% of tetrahedra satisfying the ice rule, followed by progressive thermal disordering on warming. In Ho_2TiO_5, most tetrahedra are magnetically incomplete because some tetrahedral vertices are occupied by nonmagnetic Ti rather than Ho; nevertheless, the dominant incomplete configurations are 2-in/1-out and 1-in/2-out, which are locally compatible with the ice rule if the missing Ho spin is restored. Ho_2TiO_5 is therefore a vacancy-disrupted spin ice in which the local ⟨111⟩ Ising character and short-range spin-in/spin-out correlations persist on a topologically incomplete magnetic network, while collective ice-rule correlations are strongly disrupted.

DOI: 10.1103/r2kt-8sbh

I. INTRODUCTION

Geometrically frustrated materials have been a central theme in condensed matter physics for decades, attracting intense interest due to their rich magnetic phenomena, novel ground states, and strong quantum fluctuations [1]. Geometrical magnetic frustration arises when the geometry of the crystal prevents all the competing spin interactions from being simultaneously satisfied, leading to competing ground states and often suppression of long range order while preserving local magnetic correlations. Pyrochlore titanates ($A_2Ti_2O_7$, where A = rare-earth ion) have emerged as one of the most fertile families of three-dimensional frustrated magnets. In this structure, the magnetic A-site cations sit on the vertices of a network of intrinsically frustrated corner-sharing tetrahedra. One prominent member, $Ho_2Ti_2O_7$, is a canonical spin ice material with local 2-in/2-out configurations and no long-range magnetic order down to the lowest measured temperatures [2–4]. The magnetic Ho^{3+} ion's strong crystal-electric-field environment at the A site enforces a pronounced Ising anisotropy, locking each moment to its local ⟨111⟩ direction so that it can point only toward or away from the center of a given tetrahedron [2]. As a result, the lowest-energy states satisfy the spin ice rule.

Chemical disorder provides an additional route for tuning frustration in pyrochlore oxides. Cation antisite disorder, stuffing, oxygen nonstoichiometry, and the evolution toward defect-fluorite-like local environments can modify both the connectivity of the magnetic sublattice and the local crystal-field environment without necessarily destroying the average cubic structure. Such disorder driven effects have been investigated extensively across the $A_2B_2O_7$ family and can substantially alter magnetic correlations and low-energy behavior [5–7].

The spin ice behavior of $Ho_2Ti_2O_7$ is well established. The response of this state to chemical disorder and cation stuffing has also been the subject of substantial previous work, with bulk magnetic, thermodynamic, structural, and neutron scattering measurements showing that spin ice phenomenology can persist over a broad range of stuffed compositions [8–12]. An important remaining question is how these established macroscopic signatures are reflected microscopically in the local magnetic anisotropy and tetrahedral spin correlations when the magnetic network becomes strongly incomplete. One route to create this scenario is through cation stuffing, where additional Ho ions occupy nominally nonmagnetic Ti sites and drive Ho/Ti mixing on both the A and B sublattices (see Fig. 1). This stuffing pushes the composition beyond the stoichiometric limit toward $Ho_2(Ti_{1.33}Ho_{0.67})O_{6.67}$ or simply Ho_2TiO_5. The substitution changes both the connectivity of the magnetic network and the local crystal-field environment, potentially disrupting the balance of interactions that stabilizes the ice-rule ground state.

Stuffed spin ices therefore provide a route to test the robustness of ice-rule correlations against chemical disorder and magnetic dilution. Previous work on stuffed pyrochlores has

*Contact author: baralr@ornl.gov

†Contact author: caldersa@ornl.gov

 ©2026 American Physical Society

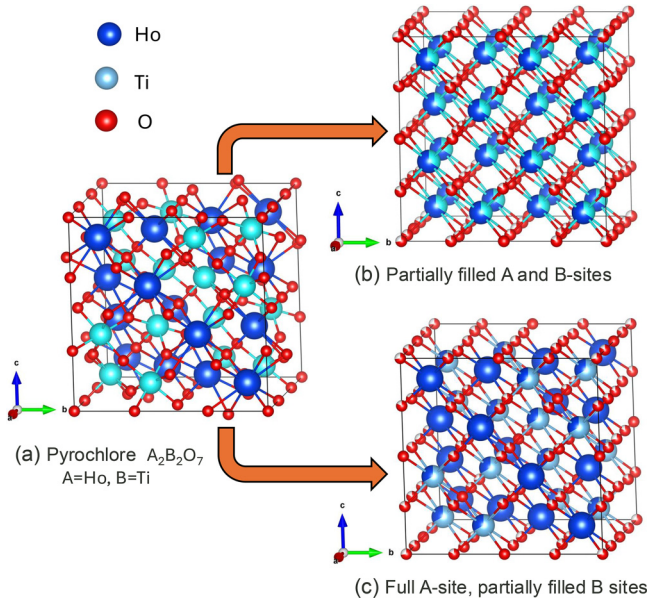


FIG. 1. Crystal structure models for pyrochlore spin ice $A_2B_2O_7$ and stuffed spin ice A_2BO_5, where A = Ho and B = Ti. (a) Pyrochlore $Ho_2Ti_2O_7$ with fully occupied A-site Ho and B-site Ti sublattices. (b) and (c) Idealized average-structure descriptions of Ho_2TiO_5 showing two possible cation-occupancy models. Panel (b) shows partial Ho occupancy on both the A and B sites, with approximately two-thirds occupancy on each sublattice. Panel (c) shows a fully occupied A site and a partially occupied B site.

shown that the average cubic symmetry can persist over a wide stuffing range, even as the local structure and magnetic response are strongly modified [8–12]. Ho_2TiO_5 represents an extreme limit of this tuning, where the average structure remains pyrochlorelike, but the local Ho/Ti network produces a large population of magnetically incomplete tetrahedra. Here, we use "vacancy" to denote a magnetic vacancy on the Ho spin network, corresponding structurally to a site occupied by nonmagnetic Ti rather than magnetic Ho. For the Ho-based stuffed spin ice series, Lau *et al.* showed from magnetization measurements that strong local Ising character persists with stuffing, while entropy measurements indicated the survival of spin-ice-like behavior across a broad composition range [8]. Subsequent neutron scattering work identified persistent ice-rule correlations in stuffed compositions [9]. The present study builds on these results by directly resolving the local susceptibility anisotropy and the real- and reciprocal-space magnetic correlations in Ho_2TiO_5.

The structural consequences of this substitution add a further layer of complexity. Depending on the synthesis conditions, the excess Ho can be accommodated in two distinct ways. One possibility is a fully occupied A site with partial occupancy of the B site. Another is simultaneous partial occupancy of both the A and B sites, with approximately two-thirds filling on each site (Fig. 1) [10–12]. These two configurations are not equivalent from a magnetic perspective, as they differ in how the Ho moments are distributed across the lattice and how vacancies interrupt the tetrahedral spin network.

Our analysis integrates a suite of complementary approaches: atomic/magnetic pair distribution function (PDF) analysis, magnetic reverse Monte Carlo (RMC) modeling, and half-polarized neutron powder diffraction (pNPD) to interrogate both the average and local atomic structures, as well as the short-range magnetic correlations, in $Ho_2Ti_2O_7$ and Ho_2TiO_5. Refinement of the average structure of Ho_2TiO_5 confirms retention of the $Fd\bar{3}m$ space group symmetry; however, systematic misfits in the low-r region of the PDF highlight the presence of local structural deviations that are not captured by long-range crystallographic descriptions. By analyzing the magnetic pair distribution function (mPDF) [13,14] and employing a magnetic reverse Monte Carlo (RMC) program SPINVERT [15] in both real and reciprocal space, we directly resolve the short-range magnetic correlations in both compounds. In $Ho_2Ti_2O_7$, the spin configurations satisfy the ice rule at low temperature, with increasing temperature leading to a progressively larger fraction of tetrahedra violating this constraint. In the stuffed spin ice Ho_2TiO_5, over 80% of tetrahedra are topologically magnetically incomplete, a direct structural consequence of the partial, 2/3-fractional occupancy of Ho^{3+} across both the A- and B-site sublattices and, among these, the dominant spin configurations are 2-in/1-out and 1-in/2-out arrangements. The remaining ∼20% of complete tetrahedra exhibit either 2-in/2-out or 3-in/1-out and 1-in/3-out configurations. This intrinsic site disorder constitutes a defining feature of stuffed spin ice and underpins the unconventional magnetic behavior observed in this system. Furthermore, our half-polarized neutron powder diffraction (pNPD) analysis confirms that the spins are constrained to point either towards or away from the center of the tetrahedra. Consequently, the single-ion ⟨111⟩ Ising anisotropy that underpins spin ice physics is retained on both sublattices, even as the topologically incomplete network strongly disrupts the collective 2-in/2-out ordering, leaving a local ice-rule tendency rather than the near-ideal local 2-in/2-out correlations realized in $Ho_2Ti_2O_7$ at low temperature.

II. EXPERIMENTAL SECTION

Powder samples of Ho_2TiO_5 and $Ho_2Ti_2O_7$ were synthesized using the solid-state reaction method, with stoichiometric amounts of dried Ho_2O_3 and TiO_2. The mixed powders were subsequently annealed in air at 1000° C, 1200° C, and 1450° C for 20 h at each temperature.

Neutron total scattering patterns of $Ho_2Ti_2O_7$ and Ho_2TiO_5 were collected on the HB-2A powder diffractometer [16] at the High Flux Isotope Reactor (HFIR) at Oak Ridge National Laboratory (ORNL). A vertically focusing germanium monochromator was used to select a wavelength of 1.12 Å from the Ge(117) reflection. The data for both samples were collected at temperatures 0.3, 1, 2, 4, 10, 20, 40, and 50 K, with a collection time of 6 h for each temperature point. The collected data were then Fourier transformed with Q_{max} = 10 $Å^{-1}$ to get the pair distribution function (PDF) data.

Half-polarized neutron powder diffraction data were also collected on HB-2A using the 2.41 Å wavelength from the Ge(113) monochromator reflection. For this data collection a polarizing supermirror V-cavity was placed in the incident beam to define a single neutron polarization state. Data were collected with the neutron spin polarization up or down with the further use of a Mezei guide-field flipper [16]. The sample

was made into pellets to avoid grain reorientation and placed in a vertical magnetic field.

Additional neutron total scattering patterns of Ho_2TiO_5 were collected at 10 and 300 K on the POWGEN powder diffractometer at the Spallation Neutron Source (SNS) at ORNL. An automatic sample changer was used as the sample environment, covering the temperature range from 10 to 300 K. Approximately 5 g of powder was loaded into an 8 mm diameter vanadium PAC can and sealed with helium exchange gas to ensure good thermal conductivity. Data were collected using a neutron frame with a center wavelength of 0.8 Å, providing d-spacing coverage of 0.1–8 Å. All the data were reduced by subtracting the signal from the empty PAC container, with normalization performed using the difference between the vanadium standard and the empty instrument background. The collected data were Fourier transformed with $Q_{max} = 30$ Å^{-1} to obtain the pair distribution function (PDF).

Atomic PDF analysis of the data was performed using the open source PYTHON package *DiffPy-CMI* [17], whereas mPDF analysis was performed using the open source PYTHON package *diffpy.mpdf* [13,14,18]. Magnetic RMC modeling was performed using the SPINVERT software [15]. Analysis of the pNPD data was performed with the open source software CRYSPY [19].

III. RESULTS AND DISCUSSION

A. Structural analysis of Ho_2TiO_5

Previous diffraction and electron-microscopy studies have already shown that Ho_2TiO_5 can retain an average pyrochlore-like structure while exhibiting substantial short-range cation and oxygen disorder [12]. PDF analysis offers a route to characterize this directly in real space and to determine the structural model appropriate for the magnetic analysis. The comparison of candidate local symmetries was additionally motivated by the PDF study of the related stuffed compound Yb_2TiO_5 by Shamblin *et al.* [20].

We begin by investigating the average and local atomic structures of Ho_2TiO_5 by utilizing PDF analysis of neutron total scattering data collected on the POWGEN instrument at 300 K. This is well above any expected magnetic correlations, allowing a focus on the solely atomic scattering. The average structural information can be obtained by fitting the PDF data at the high r region (e.g., 40–65 Å), whereas information about the local structure or any local distortion, if present, can be obtained by analyzing the low r region (e.g., 1–10 Å) of the PDF data.

To examine how the local structure evolves toward the average crystallographic structure, we performed a "*sliding-box*" refinement of the PDF data using two different structural models within the $Fd\bar{3}m$ space group: one with Ho occupancy 2/3 on both A and B sites and another with Ho occupancy 1 on the A site and 1/3 on the B site. The Ti ion fills the remaining occupancy in both models. Previous work has shown that the Ho/Ti cation distribution in Ho_2TiO_5 can depend sensitively on synthesis conditions [10]. We therefore tested both reported occupancy scenarios against our data. In this approach, the fitting range is systematically shifted to higher

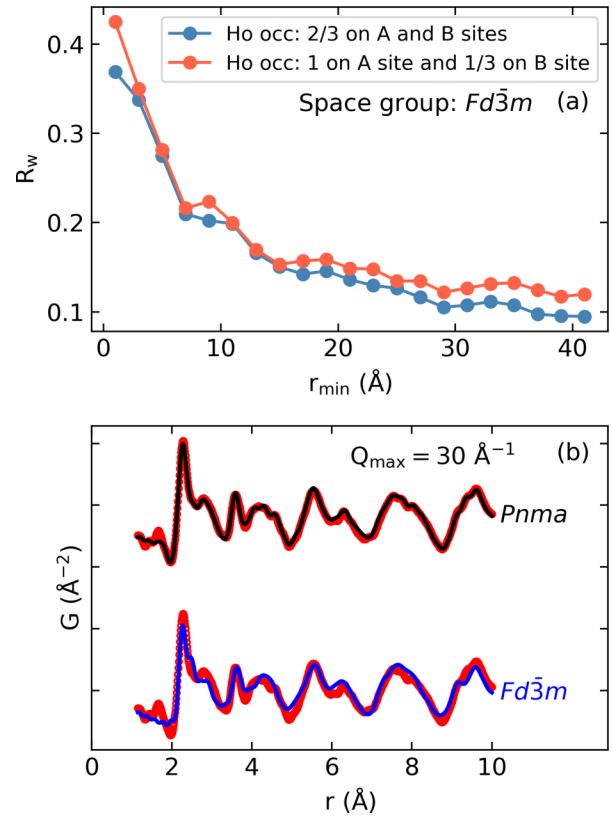


FIG. 2. (a) Goodness-of-fit parameter (R_w) as a function of minimum r value in the "*sliding-box*" refinements at 300 K. The blue symbol represents the Ho occupancy with 2/3 on both A and B sites and the orange symbol represents the Ho occupancy where the A site is fully occupied and the B site has 1/3 occupancy. (b) Local atomic fits at 300 K using the $Fd\bar{3}m$ and *Pnma* models over 1–10 Å. (Neutron scattering data collected on the POWGEN instrument.)

r values while keeping the total window width constant. Each refinement was carried out by maintaining the fitting range of 20 Å, starting from 1–21 Å for the first window, then 3–23 Å, and so on, until the final range of 41–61 Å. The goodness-of-fit parameter $R_w = \sqrt{\frac{\sum_i (y_{i,\mathrm{obs}} - y_{i,\mathrm{calc}})^2}{\sum_i (y_{i,\mathrm{obs}})^2}}$ was calculated for each refinement using the $Fd\bar{3}m$ structure. The plot of goodness-of-fit parameter (R_w) with minimum r value (r_{min}) fitting range is shown in Fig. 2(a). The R_w parameter initially decreases as the fitting range slides to higher values of r for both models. Beyond $r_{min} = 27$ Å, R_w saturates at ≈0.095 for the model with Ho occupancy 2/3 on both A and B sites and at ≈0.125 for the model with Ho occupancy 1 on the A site and 1/3 on the B site. This indicates that the average $Fd\bar{3}m$ structure better captures the high-r region of the PDF data when the 2/3 occupancy model is used. In contrast, both models fail to capture the low-r region (fitting range 1–10 Å), revealing that the local structure deviates from the average crystallographic framework [see Fig. 2(b); fit shown in blue].

The poor local structure fit motivated us to explore alternative structural models, guided by related stuffed-pyrochlore compound Yb_2TiO_5, where *Pnma* type local distortions have been reported [20]. Among $Fd\bar{3}m$, $Fm\bar{3}m$, and *Pnma*, the atomic PDF fit performed using the *Pnma* space group

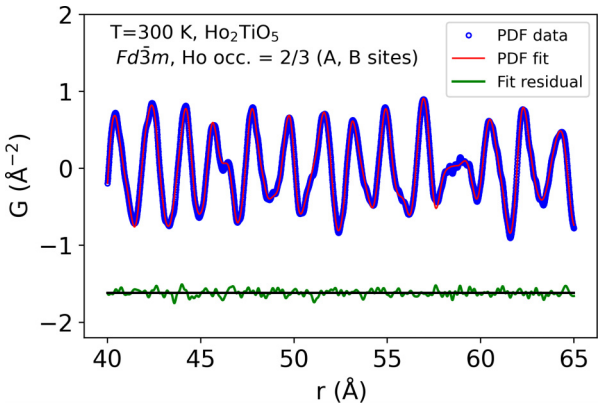


FIG. 3. PDF pattern of Ho_2TiO_5 collected on the POWGEN instrument at $T = 300$ K ($Q_{max} = 30$ Å^{-1}).

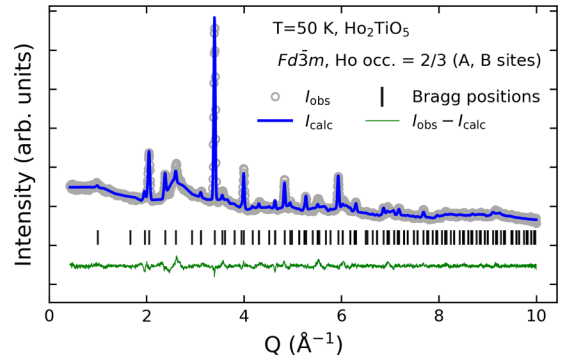


FIG. 4. Rietveld refinement of the neutron powder diffraction pattern of Ho_2TiO_5 collected at 50 K on the HB-2A instrument ($\lambda = 1.12$ Å).

reproduced the local PDF (1–10 Å), suggesting that the true local structure deviates from the average $Fd\bar{3}m$ symmetry [see Fig. 2(b)]. However, the local *Pnma* refinement contains substantially more independently refined parameters than the $Fd\bar{3}m$ model ($N_{\text{Pnma}} = 53$ compared with $N_{Fd\bar{3}m} = 15$), so the lower R_w must be interpreted cautiously because of the increased model flexibility. This concern is corroborated by the 10 K PDF data, where the *Pnma* model produces an apparently good fit, with no residual magnetic signal in the fit. Inspection of the temperature-subtracted scattering, $S(Q, 10\text{ K}) - S(Q, 50\text{ K})$, reveals a clear diffuse magnetic signal that is suppressed when the low-symmetry *Pnma* model is used. Instead, fitting to a lower-symmetry space group blends the atomic and magnetic contributions, indicating that the additional structural degrees of freedom in the *Pnma* model can absorb intensity associated with the magnetic contribution. Therefore, we do not proceed with using the *Pnma* model for the local order and instead adopt the $Fd\bar{3}m$ space group for our structural model and proceed with magnetic refinements based on this framework. The local misfits that persist at low r are accordingly interpreted as a signature of short-range Ti–O, Ho–O, and O–O bond disorder intrinsic to the stuffed pyrochlore lattice, rather than as evidence of a global symmetry breaking.

Figure 3 shows the pair distribution function (PDF) fit of Ho_2TiO_5 at $T = 300$ K over the high-r fitting range of 40–65 Å, representing the average crystal structure. The data are well reproduced by the PDF fit using the pyrochlore-type $Fd\bar{3}m$ structure with a fractional Ho occupancy of 2/3 on both the *A* and *B* sites. The flat and featureless fit residual confirms the excellent agreement between the observed and calculated PDF patterns. The quality of the fit at high r demonstrates that the $Fd\bar{3}m$ average structure model successfully captures the long-range structural correlations in Ho_2TiO_5. Details of the crystal structure are given in Table I.

The average crystal structure of Ho_2TiO_5, determined from total scattering data collected at POWGEN, is the pyrochlore-type $Fd\bar{3}m$ space group with Ho occupying both the *A* and *B* sites at 2/3 fractional occupancy, as shown in Fig. 1(b). This result is further supported by Rietveld refinement of data collected at HB-2A, which confirms mixed *A*- and *B*-site occupancy and rules out fully occupied *A* sites with 1/3 occupancy on the *B* site. A signature of the mixed occupancy can be seen by the (331) reflection being broad rather than sharp, as has been noted in previous studies [12]. Figure 4 shows the Rietveld refinement of Ho_2TiO_5 performed using the FULLPROF suite [21] at $T = 50$ K. The refinement was carried out in the pyrochlore-type $Fd\bar{3}m$ space group with a fractional Ho occupancy of 2/3 on both the Ho1 (*A* site) and Ho2 (*B* site). The background was modeled by manually selecting points in the refinement, with particular attention given to the region between 2.41 and 2.9 Å^{-1} to accurately account for the atomic diffuse scattering contribution in this range. The refinement converged with a goodness-of-fit of $\chi^2 = 2.66$, confirming the reliability of the structural model.

TABLE I. Structural parameters for Ho_2TiO_5 extracted using POWGEN PDF data at 300 K using a fitting range 40–65 Å and the space group $Fd\bar{3}m$ (no. 227). (U_{iso} = isotropic atomic displacement parameter; Occ = occupancy).

Lattice parameter: $a = 10.3008(24)$ Å

Atom	Wyckoff position	x	y	z	U_{iso}	Occ
Ho(1)	16*d*	0.5	0.5	0.5	0.0146(4)	0.667
Ti(1)	16*d*	0.5	0.5	0.5	0.0036(8)	0.333
Ho(2)	16*c*	0	0	0	0.0454(14)	0.667
Ti(2)	16*c*	0	0	0	0.0128(19)	0.333
O(1)	8*b*	0.375	0.375	0.375	0.0420(13)	1.000
O(2)	8*a*	0.125	0.125	0.125	0.0760(47)	0.730
O(3)	48*f*	0.3545(4)	0.125	0.125	0.0665(11)	0.820

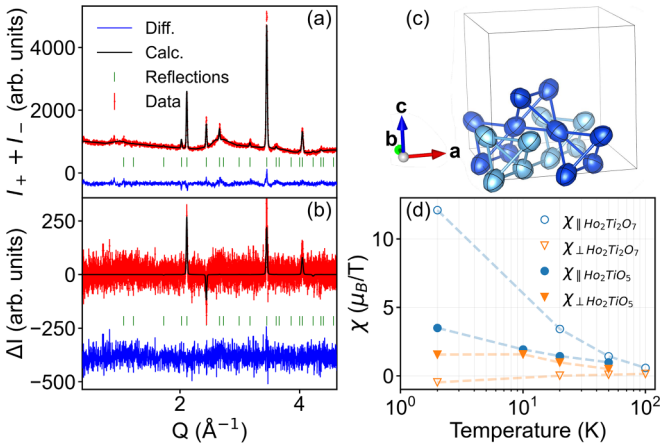


FIG. 5. Half-polarized neutron powder diffraction for the (a) sum and (b) difference (ΔI) of I_+ and I_- measurements of Ho_2TiO_5 at 10 K and $H = 0.5$ T. (c) Local susceptibility ellipsoids for the Ho ions extracted from the model fits. (d) Parallel ($\chi_\parallel$) and perpendicular ($\chi_\perp$) components of the susceptibility as a function of temperature for Ho_2TiO_5 at $H = 1.5$ T compared to $Ho_2Ti_2O_7$ at $H = 1$ T. (Neutron scattering data collected on the HB-2A instrument.)

B. Local site susceptibility measurements of Ho_2TiO_5

To investigate the local magnetic anisotropy in Ho_2TiO_5, pNPD measurements were performed. This technique, described in detail in Ref. [22], uses two measurements with the incident neutron beam polarization parallel (I_+) or antiparallel (I_-) to an applied magnetic field at the sample position. Data were collected at 10 K in an applied field of 0.5 T, within the linear M/H regime [10]. Both datasets were modeled using the CrysPy software [19] to extract the local site susceptibility tensor; see Figs. 5(a) and 5(b). The Ho ions were assumed to be randomly distributed on both Ho1/Ti1 and Ho2/Ti2 sites with 2/3 occupancy on each.

A key question for the stuffed pyrochlore Ho_2TiO_5 is whether the B-site Ho^{3+} ions on the nominal B sublattice, which is sixfold coordinated in the ideal parent pyrochlore rather than eightfold coordinated as on the A sublattice, retain a local ⟨111⟩ easy-axis preference. To address this, models were tested with both independent (unconstrained) and equal (Ho1=Ho2) susceptibility tensors. In the unconstrained refinement, both sites independently exhibit uniaxial anisotropy with the easy axis along the local ⟨111⟩ direction and quantitatively similar principal values: $\chi_\parallel = 3.80\mu_B$/T and $\chi_\perp = 1.82\mu_B$/T for the A-site Ho1 and $\chi_\parallel = 4.08\mu_B$/T and $\chi_\perp = 1.85\mu_B$/T for the B-site Ho2. Despite the distinct crystallographic coordination environments, the B-site Ho moments are not differently oriented; they carry comparable ⟨111⟩ Ising anisotropy to the A-site Ho. This provides experimental evidence that the spin correlations develop along the local ⟨111⟩ directions across both magnetic sublattices.

Given the close agreement between the two sites, the constrained model (Ho1=Ho2) was adopted for final quantitative analysis. The resulting susceptibility tensor at 10 K and 0.5 T is

$$\chi_{\mathrm{Ho}} = \begin{pmatrix} 2.3(2) & 0.7(4) & 0.7(4) \\ 0.7(4) & 2.3(2) & 0.7(4) \\ 0.7(4) & 0.7(4) & 2.3(2) \end{pmatrix} \mu_B/\mathrm{T}.$$

The corresponding susceptibility ellipsoids are shown in Fig. 5(c). The easy axis points into or out of the center of the tetrahedra for both the Ho1 and Ho2 sublattices, confirming that the single-ion anisotropy required for spin ice physics is preserved across the entire Ho network. Although the ⟨111⟩ easy axis is retained, the anisotropy ratio $\chi_\parallel/\chi_\perp \approx 2.3$ is reduced from the sharp Ising limit observed in $Ho_2Ti_2O_7$, consistent with a larger transverse susceptibility arising from the modified crystal-field environment due to cation mixing and oxygen vacancies in the stuffed lattice. Thus the local ⟨111⟩ easy-axis direction survives on the B-site Ho despite its strongly modified oxygen coordination, but the appreciable transverse susceptibility shows that the anisotropy is softer than the nearly ideal Ising limit of $Ho_2Ti_2O_7$. We attribute the softening of the anisotropy to the distribution of local crystal-field environments generated by Ho/Ti disorder and oxygen vacancies.

To further quantify how disorder affects the anisotropy, we compare the temperature dependent $\chi_\parallel$ and $\chi_\perp$ values for Ho_2TiO_5 with those reported for $Ho_2Ti_2O_7$ in Ref. [16] [Fig. 5(d)]. At low temperature, clear anisotropy is present in both compounds, with the easy axis promoting spins to point into or out of the tetrahedra. However, this anisotropy is damped significantly more rapidly with increasing temperature in Ho_2TiO_5 than in $Ho_2Ti_2O_7$, analogous to how thermal fluctuations soften the Ising character in the parent compound, but occurring at a lower energy scale due to the structural disorder. The retention of ⟨111⟩ Ising anisotropy on both cation sublattices establishes that the single-ion prerequisite for spin ice correlations survives the stuffing process and that the disruption of ice-rule order in Ho_2TiO_5 arises from the incomplete tetrahedral connectivity rather than a loss of the underlying Ising character.

C. Magnetic pair distribution function analysis

With an understanding of the anisotropy of the spins in both $Ho_2Ti_2O_7$ and Ho_2TiO_5 we now turn to probing the magnetic correlations, which remain short range down to the lowest temperatures measured in zero field in both materials. mPDF offers a route to investigate short range order in real space. We begin with $Ho_2Ti_2O_7$ as a reference; however, we note that direct analysis of mPDF models against data does not appear in the literature for $Ho_2Ti_2O_7$. We then extend our treatment of mPDF analysis to Ho_2TiO_5.

1. mPDF analysis of $Ho_2Ti_2O_7$

We analyzed the short-range magnetic correlations of $Ho_2Ti_2O_7$ in real space using the mPDF technique. The magnetic PDF signal was isolated by first performing an atomic PDF refinement using the established $Fd\bar{3}m$ crystal structure of $Ho_2Ti_2O_7$. The resulting fit residual, defined as the difference between the measured PDF and the calculated atomic PDF, was then subjected to temperature subtraction in real space, using the atomic fit residual of 50 K data as a reference, following the approach described in Ref. [23]. The 50 K dataset was used as the highest-temperature reference available for the subtraction. The resulting mPDF signal was subsequently used as input for the mPDF refinement. For $Ho_2Ti_2O_7$, weak short-range magnetic correlations may

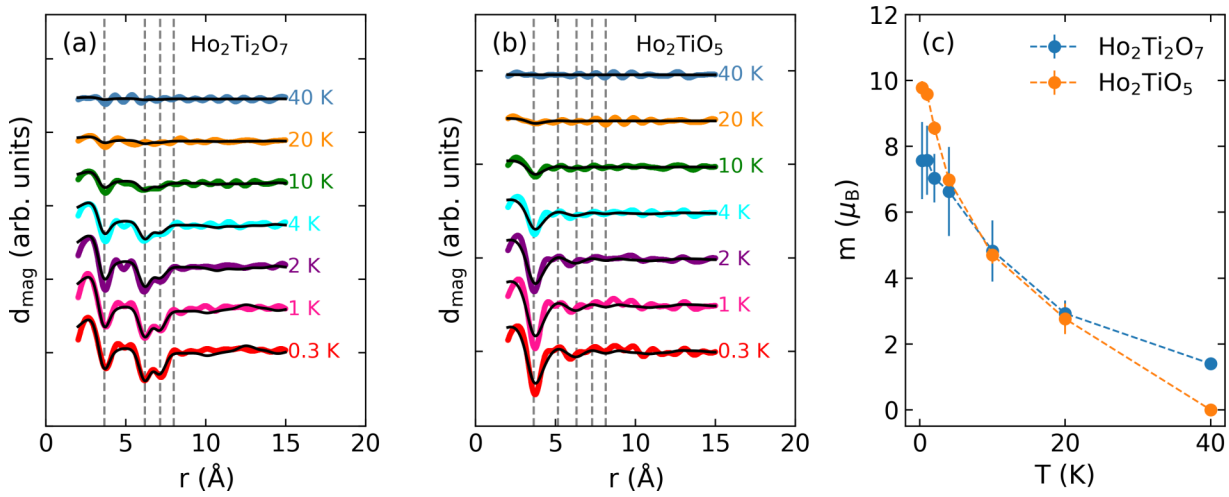


FIG. 6. Temperature dependent mPDF fits of (a) $Ho_2Ti_2O_7$ and (b) Ho_2TiO_5. The mPDF patterns are vertically offset for clarity. A Fourier filter was applied to smooth the experimental signal, removing contributions above 6.5 $Å^{-1}$; this cutoff is justified by the magnetic form factor, which causes the magnetic scattering intensity to become negligible at higher Q. (c) Temperature dependence of the Ho mPDF moment amplitude extracted from mPDF fits for $Ho_2Ti_2O_7$ and Ho_2TiO_5. (Neutron scattering data collected on the HB-2A instrument.)

persist at 50 K, so this procedure can remove a small amount of magnetic scattering together with the nonmagnetic background.

Figure 6(a) shows the mPDF refinement of $Ho_2Ti_2O_7$ at various temperatures. At 0.3 K, a pronounced negative peak is observed at the nearest-neighbor distance of ≈3.57 Å, reflecting the expected nearest-neighbor correlation for 2-in/2-out configurations on a tetrahedron in the global spin basis. Two additional negative peaks appear at ≈6.18 Å and ≈7.14 Å, corresponding to the second and third nearest-neighbor distances, respectively. The magnetic model captures all three peaks well, though the agreement diminishes at larger distances as the peaks become progressively weaker. This behavior indicates that nonrandom spin correlations persist up to a length scale of approximately 7–8 Å at 0.3 K. The small negative feature at ∼5 Å is a Fourier-truncation artifact, not a genuine feature. It does not correspond to any Ho–Ho distance in the structure and cannot be magnetic in origin.

In order to perform the mPDF refinement of $Ho_2Ti_2O_7$ a custom Python script was used to generate a 2-in/2-out spin configuration. The resulting spin configuration was used to perform mPDF refinement and the local magnetic moment was calculated. As 2-in/2-out spin configuration can be realized through multiple distinct spin arrangements, the refinement was repeated over several independent configurations and the resulting local moments were averaged to obtain a statistically robust value.

2. *mPDF analysis of* Ho_2TiO_5

Having established the crystal structure and local magnetic anisotropy of Ho_2TiO_5 above, and with the example of $Ho_2Ti_2O_7$, we now turn to the analysis of the short range magnetic correlations at low temperature directly in real space using the mPDF technique for Ho_2TiO_5. The isolation of the magnetic PDF signal was done in a similar manner to $Ho_2Ti_2O_7$ using $Fd\bar{3}m$ space group with Ho occupancy 2/3 on both A and B sites. The atomic PDF fits were performed over the temperature range 0.3–50 K. The 50 K atomic fit residual was subtracted from the residual at each lower temperature in real space [23] to get a clean mPDF signal which was used as input for the mPDF refinement. $Ho_2Ti_2O_7$ was first used as a reference to establish the mPDF refinement, where Ho site (Ho on A site) follows a perfect 2-in/2-out spin ice configuration. Since Ho_2TiO_5 has a fractional occupancy of 2/3 on both the A and B sites, the 2-in/2-out model was extended to include both sites, using the $Ho_2Ti_2O_7$ refinement as the starting point.

Figure 6(b) shows the mPDF refinements of Ho_2TiO_5 at various temperatures using the spin ice structural model. At 0.3 K, a pronounced negative nearest-neighbor mPDF peak at ≈3.6 Å reflects the expected relative orientation of neighboring Ho moments in the local spin-in/spin-out configurations on a tetrahedron. The negative sign of this nearest-neighbor mPDF peak reflects the geometrical spin-pair correlation in the global spin basis and should not be interpreted as evidence for antiferromagnetic exchange. A two-in/two-out spin ice configuration can produce an antiferromagneticlike nearest-neighbor mPDF correlation even when the effective interaction stabilizing the spin ice state is ferromagnetic [14].

The second-neighbor correlation produces a positive peak at ≈5.14 Å. The positive feature at ≈5.14 Å arises from an Ho(A)–Ho(B) pair introduced by the partial occupation of the nominal Ti sublattice by Ho. This pair is absent in stoichiometric $Ho_2Ti_2O_7$, in which Ho occupies only the conventional pyrochlore A sublattice. Similarly, the third-neighbor correlation produces a negative peak at ≈6.3 Å. The magnetic model captures all three peaks well, although the agreement diminishes at larger distances as the peaks become progressively weaker. This behavior indicates that nonrandom spin correlations persist over a length scale of approximately 6–7 Å at 0.3 K.

A series of mPDF fits were performed for $Ho_2Ti_2O_7$ and Ho_2TiO_5 over the fitting range 2–15 Å. The refined mPDF scale was converted to an effective correlated moment amplitude, which tracks the strength of the finite-range magnetic

correlations but should not be interpreted as the full ionic Ho^{3+} moment or as a long-range ordered moment. These values are shown in Fig. 6(c). At 0.3 K, the fitted amplitudes are approximately $7.6\mu_B$ for $Ho_2Ti_2O_7$ and $9.7\mu_B$ for Ho_2TiO_5. The lower absolute value obtained for $Ho_2Ti_2O_7$ is likely influenced by the use of the 50 K dataset as the subtraction reference, since residual short-range correlations may persist at that temperature and would therefore be partially removed. The absolute amplitudes should consequently be interpreted with caution, while their temperature dependence provides a measure of the evolution of the correlated magnetic signal.

With increasing temperature, the effective correlated moment decreases monotonically in both compositions, consistent with thermal disordering of the local spin configurations. Notably, at 40 K the effective moment in $Ho_2Ti_2O_7$ remains finite at $\sim 1.5\mu_B$, whereas that of Ho_2TiO_5 approaches zero, indicating the absence of detectable short-range magnetic correlations above this temperature within the sensitivity of the present mPDF analysis. This difference in energy scale is consistent with the stronger disruption of spin ice correlations by Ho/vacancy disorder in Ho_2TiO_5.

IV. REVERSE MONTE CARLO MODELING OF DIFFUSE MAGNETIC SCATTERING

To form a complete picture of the microscopic magnetism in Ho_2TiO_5 we extend our investigation by combining both reciprocal-space and real-space analysis methods, as has been shown to be advantageous in studies of short-range magnetic order in frustrated magnets [24]. In reciprocal space the reverse Monte Carlo (RMC) technique was implemented in SPINVERT to analyze the broad diffuse magnetic scattering that is observed with decreasing temperature in Ho_2TiO_5 and $Ho_2Ti_2O_7$, without any transition to long range magnetic order. This methodology allows for a model independent testing of spin arrangements, both within the anisotropic constraints of spins pointing in/out of tetrahedra and for unconstrained spins. We use $Ho_2Ti_2O_7$ as a reference and extend this to Ho_2TiO_5.

RMC modeling of $Ho_2Ti_2O_7$. Prior to RMC modeling of the magnetic scattering in the neutron diffraction data of $Ho_2Ti_2O_7$, the magnetic signal was isolated from the nuclear contribution. Bragg peaks were identified and removed from the powder dataset using an automated PYTHON algorithm [25], leaving only the diffuse magnetic scattering component. Thus extracted diffuse magnetic scattering components were subsequently normalized to absolute intensity [26] and then RMC refinements were carried out using SPINVERT software. For RMC calculations, we defined a $5 \times 5 \times 5$ supercell and 100 independent RMC refinements were performed and averaged to improve statistical reliability.

The RMC fit for $Ho_2Ti_2O_7$ at 0.3 K is shown in Fig. 7(b). The RMC fit demonstrates good agreement between the model and the data across the measured Q range. Analysis of the refined spin structure of $Ho_2Ti_2O_7$ at 0.3 K reveals that approximately 95% of tetrahedra satisfy the 2-in/2-out ice rule, while the remaining approximately 5% adopt 3-in/1-out or 1-in/3-out configurations.

Similar RMC refinements were performed across the full temperature range from 0.3 to 40 K. Figure 7(c) shows the

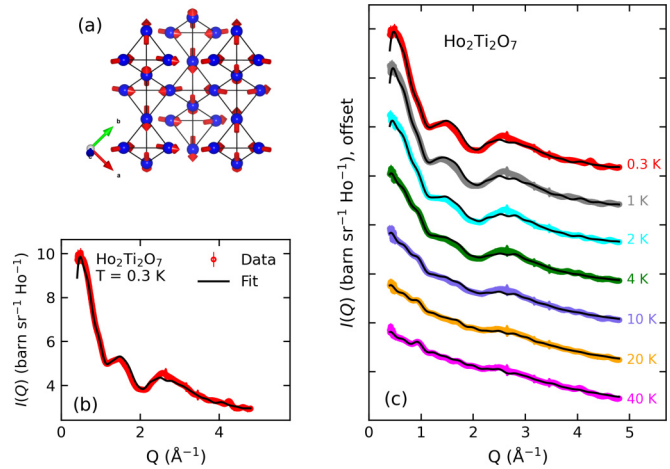


FIG. 7. (a) 2-in/2-out spin structure. (b) Reverse Monte Carlo (RMC) modeling of the magnetic diffuse scattering of $Ho_2Ti_2O_7$ at 0.3 K using SPINVERT. The red symbols represent the experimental magnetic diffuse scattering data, while the black line shows the SPINVERT fit. (c) Vertically stacked temperature series of magnetic diffuse scattering data (colored curves) in Q space with their respective SPINVERT fit (black line). (Neutron scattering data collected on the HB-2A instrument.)

SPINVERT fit of the whole temperature series and resulting spin configuration fractions are summarized in Fig. 8. The ice rule compliance remains dominant at low temperatures, with approximately 95% of tetrahedra satisfying the 2-in/2-out condition at 0.3, 1, and 2 K. As the temperature increases, the fraction of ice-rule-obeying tetrahedra decreases monotonically, accompanied by a corresponding increase in the 3-in/1-out, 1-in/3-out, and all-in/all-out population. At 20 K and above, the two spin configurations (2-in/2-out and 3-in/1-out or 1-in/3-out) are present in nearly equal proportions, indicating a progressive breakdown of spin ice correlations with increasing thermal fluctuations (see Fig. 8).

RMC modeling of Ho_2TiO_5. To investigate the nature of the magnetic diffuse scattering and its evolution with

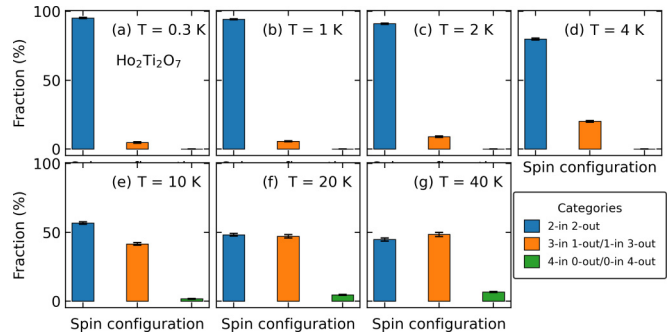


FIG. 8. Bar charts showing the fraction of tetrahedra adopting each spin configuration as a function of temperature for $Ho_2Ti_2O_7$ obtained from RMC refinements. Blue, orange, and green bars represent the 2-in/2-out, 3-in/1-out or 1-in/3-out, and 4-in/0-out or 0-in/4-out spin configurations, respectively. Error bars denote the standard deviation over 100 independent RMC refinements.

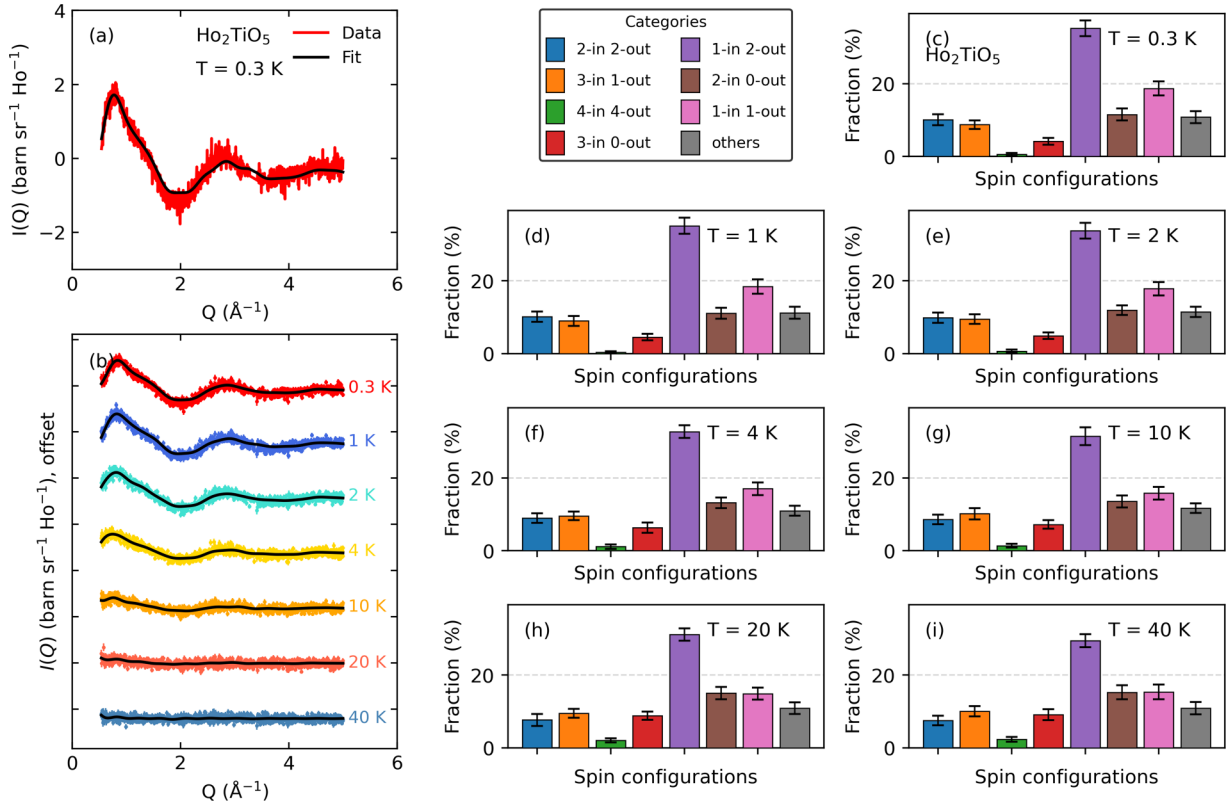


FIG. 9. (a) RMC fit to the magnetic diffuse scattering of Ho_2TiO_5 at 0.3 K. Red symbols show the data and the black line shows the fit. (b) Temperature series of RMC fits, vertically offset for clarity. (c)–(i) Fractions of tetrahedral spin configurations extracted from the RMC refinements as a function of temperature. Colors denote 2-in/2-out, 3-in/1-out or 1-in/3-out, 4-in/0-out or 0-in/4-out, 3-in/0-out or 0-in/3-out, 2-in/1-out or 1-in/2-out, 2-in/0-out or 0-in/2-out, 1-in/1-out, and single-spin configurations. (Neutron scattering data collected on the HB-2A instrument.)

temperature, RMC refinements were performed against the total neutron scattering data of polycrystalline Ho_2TiO_5 collected at temperatures ranging from 0.3 K to 50 K. To isolate the diffuse magnetic signal a temperature subtraction approach was employed. The 50 K dataset, where magnetic correlations are negligible, was used as a reference and subtracted from all lower-temperature datasets. The resulting difference patterns contain the isolated magnetic diffuse scattering, which was then modeled using SPINVERT.

The magnetic RMC analysis of Ho_2TiO_5 was carried out using SPINVERT based on the average $Fd\bar{3}m$ structure, employing a $5 \times 5 \times 5$ supercell with fractional occupancies of 2/3 for both the Ho1 (*A* site) and Ho2 (*B* site). Vacancies were introduced by randomly removing Ho atoms from both sites to match the 2/3 occupancy and this process was repeated 100 times with different random vacancy configurations to ensure a well-converged statistical ensemble. Two different refinement approaches were performed: spins constrained along the local ⟨111⟩ directions (into or out of the Ho^{3+} tetrahedra) and spins freely rotating in three dimensions. While both yielded comparable fit quality, the unconstrained model produced randomly oriented spins with no physically meaningful correlations, indicative of overfitting. All subsequent analyses were therefore performed with the ⟨111⟩ Ising constraint, consistent with the established single-ion anisotropy of Ho^{3+} in the pyrochlore environment and the pNPD results presented above for the local anisotropy.

Figure 9(a) shows the SPINVERT fit of the 0.3 K data of Ho_2TiO_5, demonstrating excellent agreement between the RMC model and the experimental diffuse scattering across the measured Q range. Figure 9(b) presents the SPINVERT fits at all measured temperatures, where the data are vertically offset for clarity. The quality of the fits across the full temperature range confirms the reliability of the extracted spin configurations and allows a systematic investigation of how the diffuse magnetic correlations evolve with temperature in this material.

The RMC modeling of Ho_2TiO_5 at 0.3 K data reveals distinctions when contrasted against the canonical spin ice behavior observed in $Ho_2Ti_2O_7$. Figures 9(c)–9(i) show the fractions of spin configurations for the temperature series. Approximately 20% of tetrahedra are magnetically complete, in agreement with the value $(2/3)^4 \approx 0.20$ expected for random 2/3 occupancy of the four tetrahedral vertices, while the remaining ∼80% contain at least one vacancy. Out of 20% complete tetrahedra only 10% follow the classical 2-in/2-out spin configuration, whereas 9% follow the 3-in 1-out or 1-in 3-out spin configuration and about 1% follow an all-in/all-out spin configuration. This stands in sharp contrast to $Ho_2Ti_2O_7$, where the 2-in/2-out spin configuration accounts for ∼95% of tetrahedra, indicating that the spin ice correlations are significantly disrupted in Ho_2TiO_5. Even at 0.3 K, the complete tetrahedra do not exclusively adopt the 2-in/2-out configuration. Renormalizing the complete-tetrahedron populations gives approximately 50% 2-in/2-out,

45% 3-in/1-out or 1-in/3-out, and 5% all-in/all-out, compared with 37.5%, 50%, and 12.5% expected for randomly oriented Ising spins on a complete tetrahedron. The complete tetrahedra therefore retain a measurable ice-rule preference, with 2-in/2-out enhanced and all-in/all-out suppressed relative to the random-spin limit, although this preference is far weaker than the ∼95% ice-rule compliance of $Ho_2Ti_2O_7$. We attribute the weakened ice-rule preference to the corner-sharing connectivity of the pyrochlorelike network: although a given tetrahedron may itself be magnetically complete, it shares corners with neighboring tetrahedra that are frequently disrupted by vacancies, modifying the magnetic connectivity and the collective constraints that stabilize the 2-in/2-out state in $Ho_2Ti_2O_7$. This behavior is consistent with short-range spin-ice-like correlations that are strongly disrupted by vacancies rather than the near-ideal local ice-rule state of $Ho_2Ti_2O_7$.

A large population (80%) of tetrahedra are partially occupied in Ho_2TiO_5. Among those the most common configurations are 1-in 2-out or 2-in 1-out spin configurations. These incomplete configurations are compatible with locally spin-ice-like arrangements in the sense that restoring the missing spin with the appropriate orientation would yield a 2-in/2-out tetrahedron; we do not, however, interpret their predominance as independent evidence for an ice-rule preference, since these configurations are also the majority outcome for randomly oriented Ising spins on a three-site tetrahedron. The clearest evidence for surviving spin ice correlations is instead the retained ⟨111⟩ anisotropy, the mPDF nearest-neighbor correlations, and the ice-rule enhancement on the complete tetrahedra. The remaining incomplete tetrahedra are 3-in 0-out or vice versa, 2-in 0-out or vice versa, 1-in 1-out, and single spin tetrahedra [see Fig. 9(c)]. These results indicate that Ho_2TiO_5 does not exhibit fully well-defined spin ice order characteristics compared to $Ho_2Ti_2O_7$, but instead the local spin correlations remain compatible with spin-ice-like arrangements while being strongly disrupted by magnetic vacancies arising from Ti occupation. The system can therefore be described as a *vacancy-disrupted spin ice*, in which the geometric frustration inherent to the underlying tetrahedral motif competes with the disorder introduced by the nonstoichiometric holmium site occupancy.

Unlike $Ho_2Ti_2O_7$, where warming produces a pronounced transfer of population from 2-in/2-out configurations into 3-in/1-out and 1-in/3-out configurations, the configuration fractions in Ho_2TiO_5 show only weak temperature dependence over the measured range. This suggests that the dominant limitation on ice-rule order in Ho_2TiO_5 is not thermal population of monopolelike defects, but the quenched Ho/Ti disorder that fixes a large fraction of the tetrahedra in magnetically incomplete configurations. The temperature dependence is instead more clearly reflected in the weakening of the diffuse-scattering intensity and the mPDF amplitude.

V. CONCLUSION

In conclusion, we have combined neutron total scattering, mPDF analysis, reciprocal-space RMC modeling, and half-polarized neutron powder diffraction to determine how local spin ice correlations evolve from the classical pyrochlore spin ice $Ho_2Ti_2O_7$ to the vacancy-disrupted stuffed compound Ho_2TiO_5. Both compounds retain $Fd\bar{3}m$ symmetry at the average structural level. In Ho_2TiO_5, however, this average description does not fully capture the local structure. The low-r PDF misfit is consistent with short-range Ho–O, Ti–O, and O–O bond-length disorder associated with partial Ho/Ti occupancy, rather than a true symmetry-lowering transition.

Despite this structural disorder, Ho_2TiO_5 retains the local ingredients of spin ice physics, including ⟨111⟩ Ising anisotropy and short-range spin-in/spin-out correlations. The diffuse scattering and mPDF results show that the Ho moments retain local spin-in/spin-out correlations on the tetrahedral network. This interpretation is supported by half-polarized neutron powder diffraction, which shows that the local ⟨111⟩ Ising anisotropy is preserved even in the disordered stuffed lattice. The anisotropy is reduced relative to the strong Ising limit of $Ho_2Ti_2O_7$, consistent with a distribution of local crystal-field environments around the Ho ions.

For the reference spin ice $Ho_2Ti_2O_7$, RMC and mPDF analyses reveal a nearly ideal 2-in/2-out state at base temperature, with approximately 95% of tetrahedra obeying the spin ice rule. Upon warming, this local ice-rule order progressively weakens, as an increasing fraction of tetrahedra adopt monopolelike three-in/one-out or one-in/three-out configurations. This behavior provides a benchmark for identifying the effects of vacancy disorder in Ho_2TiO_5.

In Ho_2TiO_5, the partial Ho occupancy produces a topologically incomplete magnetic network in which most tetrahedra contain one or more vacant magnetic sites. Nevertheless, the dominant incomplete configurations are 2-in/1-out and 1-in/2-out, which are locally compatible with the spin ice rule if the vacant site is restored. Thus Ho_2TiO_5 is not simply a disorder destroyed spin ice. Instead, it realizes a vacancy-disrupted spin ice in which the local ⟨111⟩ Ising anisotropy and short-range spin-in/spin-out correlations survive on an incomplete tetrahedral network, while collective ice-rule correlations are strongly degraded. These results show that the single-ion prerequisites for spin ice physics can survive strong magnetic dilution while the collective ice-rule ordering is substantially degraded, providing a microscopic picture of how structural disorder reshapes frustration rather than simply destroying it.

ACKNOWLEDGMENTS

This research used resources at the High Flux Isotope Reactor and Spallation Neutron Source, a DOE Office of Science User Facility operated by Oak Ridge National Laboratory. Beam time was allocated on HB-2A (POWDER) under Proposals No. IPTS-31471 and No. IPTS-31582 and on POWGEN under Proposal No. IPTS-34824. The sample synthesis (H.Z.) was supported by the U.S. Department of Energy (DOE) under Grant No. DE-SC0020254. B.A.F. was supported by the U.S. National Science Foundation, Division of Materials Research, LEAPS-MPS program through Award No. 2418438. We thank J. Paddison for helpful discussions on magnetic RMC modeling.

DATA AVAILABILITY

The data that support the findings of this study are available from the corresponding authors upon reasonable request.

[1] J. S. Gardner, M. J. P. Gingras, and J. E. Greedan, Magnetic pyrochlore oxides, Rev. Mod. Phys. **82**, 53 (2010).

[2] M. J. Harris, S. T. Bramwell, D. F. McMorrow, T. Zeiske, and K. W. Godfrey, Geometrical frustration in the ferromagnetic pyrochlore $Ho_2Ti_2O_7$, Phys. Rev. Lett. **79**, 2554 (1997).

[3] S. T. Bramwell and M. J. Harris, Frustration in Ising-type spin models on the pyrochlore lattice, J. Phys.: Condens. Matter **10**, L215 (1998).

[4] S. T. Bramwell, M. J. Harris, B. C. den Hertog, M. J. P. Gingras, J. S. Gardner, D. F. McMorrow, A. R. Wildes, A. Cornelius, J. D. M. Champion, R. G. Melko, and T. Fennell, Spin correlations in $Ho_2Ti_2O_7$: A dipolar spin ice system, Phys. Rev. Lett. **87**, 047205 (2001).

[5] H. Takatsu, S. Onoda, S. Kittaka, A. Kasahara, Y. Kono, T. Sakakibara, Y. Kato, B. Fåk, J. Ollivier, J. W. Lynn, T. Taniguchi, M. Wakita, and H. Kadowaki, Quadrupole order in the frustrated pyrochlore $Tb_{2+x}Ti_{2-x}O_{7+y}$, Phys. Rev. Lett. **116**, 217201 (2016).

[6] O. Benton, Instabilities of a U(1) quantum spin liquid in disordered non-Kramers pyrochlores, Phys. Rev. Lett. **121**, 037203 (2018).

[7] V. Porée, E. Lhotel, S. Petit, A. Krajewska, P. Puphal, A. H. Clark, V. Pomjakushin, H. C. Walker, N. Gauthier, D. J. Gawryluk, and R. Sibille, Crystal-field states and defect levels in candidate quantum spin ice $Ce_2Hf_2O_7$, Phys. Rev. Mater. **6**, 044406 (2022).

[8] G. C. Lau, R. S. Freitas, B. G. Ueland, B. D. Muegge, E. L. Duncan, P. Schiffer, and R. J. Cava, Zero-point entropy in stuffed spin-ice, Nat. Phys. **2**, 249 (2006).

[9] R. J. Aldus, T. Fennell, P. P. Deen, E. Ressouche, G. C. Lau, R. J. Cava, and S. T. Bramwell, Ice rule correlations in stuffed spin ice, New J. Phys. **15**, 013022 (2013).

[10] G. C. Lau, R. S. Freitas, B. G. Ueland, M. L. Dahlberg, Q. Huang, H. W. Zandbergen, P. Schiffer, and R. J. Cava, Structural disorder and properties of the stuffed pyrochlore Ho_2TiO_5, Phys. Rev. B **76**, 054430 (2007).

[11] G. Lau, B. Muegge, T. McQueen, E. Duncan, and R. Cava, Stuffed rare earth pyrochlore solid solutions, J. Solid State Chem. **179**, 3126 (2006).

[12] G. Lau, T. McQueen, Q. Huang, H. Zandbergen, and R. Cava, Long- and short-range order in stuffed titanate pyrochlores, J. Solid State Chem. **181**, 45 (2008).

[13] B. A. Frandsen and S. J. L. Billinge, Magnetic structure determination from the magnetic pair distribution function (mPDF): Ground state of MnO, Acta Cryst. A **71**, 325 (2015).

[14] B. A. Frandsen, X. Yang, and S. J. L. Billinge, Magnetic pair distribution function analysis of local magnetic correlations, Acta Cryst. A **70**, 3 (2014).

[15] J. A. M. Paddison, J. Ross Stewart, and A. L. Goodwin, Spinvert: A program for refinement of paramagnetic diffuse scattering data, J. Phys.: Condens. Matter **25**, 454220 (2013).

[16] R. Baral, D. R. Yahne, M. J. Cochran, M. Powell, J. W. Kolis, H. Zhou, and S. Calder, Magnetic pair distribution function and half polarized neutron powder diffraction at the HB-2A powder diffractometer, J. Magn. Magn. Mater. **630**, 173342 (2025).

[17] P. Juhás, C. L. Farrow, X. Yang, K. R. Knox, and S. J. L. Billinge, Complex modeling: A strategy and software program for combining multiple information sources to solve ill-posed structure and nanostructure inverse problems, Acta Cryst. A **71**, 562 (2015).

[18] B. A. Frandsen, P. K. Hamilton, J. A. Christensen, E. Stubben, and S. J. L. Billinge, *diffpy.mpdf*: Open-source software for magnetic pair distribution function analysis, J. Appl. Cryst. **55**, 1377 (2022).

[19] I. Kibalin, A. Sazonov, and A. Gukasov, Cryspy: A software for polarized neutron diffraction data analysis, Github, 2024, https://github.com/ikibalin/cryspy.

[20] J. Shamblin, Z. Dun, M. Lee, S. Johnston, E. S. Choi, K. Page, Y. Qiu, and H. Zhou, Structural and magnetic short-range order in fluorite Yb_2TiO_5, Phys. Rev. B **96**, 174418 (2017).

[21] J. Rodríguez-Carvajal, Recent advances in magnetic structure determination by neutron powder diffraction, Physica B **192**, 55 (1993).

[22] I. A. Kibalin and A. Gukasov, Local magnetic anisotropy by polarized neutron powder diffraction: Application of magnetically induced preferred crystallite orientation, Phys. Rev. Res. **1**, 033100 (2019).

[23] B. Jones, C. Z. Suggs, E. Krivyakina, D. Phelan, V. O. Garlea, O. Chmaissem, and B. A. Frandsen, Local atomic and magnetic structure of multiferroic (Sr, Ba)(Mn, Ti)O_3, Phys. Rev. B **109**, 024423 (2024).

[24] K. M. Nuttall, C. Z. Suggs, H. E. Fischer, M. M. Bordelon, S. D. Wilson, and B. A. Frandsen, Quantitative investigation of the short-range magnetic correlations in the candidate quantum spin liquid $NaYbO_2$, Phys. Rev. B **108**, L140411 (2023).

[25] S. R. Hatt, C. Shaw, E. Zappala, R. Baral, S. Calder, G. D. Morris, B. R. Ortiz, K. Chesnel, and B. A. Frandsen, Cluster spin glass correlations and dynamics in $Zn_{0.5}Mn_{0.5}Te$, Phys. Rev. B **112**, 144440 (2025).

[26] J. A. M. Paddison, Absolute intensity normalization of powder neutron scattering data, J. Appl. Cryst. **58**, 1022 (2025).